PFC/JA-92-22

A Series Expansion Method in Three Dimensional Tomography

Ling Wang and Robert S. Granetz

Plasma Fusion Center
Massachusetts Institute of Technology
Cambridge, MA 02139

August, 1992

Submitted to Journal of Optical Society of America A.

This work was supported by the U. S. Department of Energy Contract No. DE-AC02-78ET51013. Reproduction, translation, publication, use and disposal, in whole or in part by or for the United States government is permitted.

A Series Expansion Method in Three Dimensional Tomography

Ling Wang and Robert S. Granetz

Plasma Fusion Center

Massachusetts Institute of Technology

Cambridge, MA02139

United States of America

Abbreviated title:

A Series Expansion Method in 3-D Tomography

Key words. X-ray transform, three dimensional tomography, spherical harmonic series expansion, Euler angles.

AMS(MOS) subject classifications. 44A15,42C15

ABSTRACT

A series expansion method in three dimensional tomography is presented. While the function to be reconstructed is expanded in terms of spherical harmonics and orthogonal polynomials, the projection of the function is expanded in terms of Euler angles in the angular part and orthogonal polynomials in the radial part. The computer simulation of the reconstruction demonstrates the applicability of the method.

1. Introduction

In two dimensional tomography since the pioneering work of Cormack [1], the method of series expansion in terms of Fourier harmonics is well known to have great advantages when the number of views is limited. Deans has given an extensive review of the method and its applications in many branches of science and engineering [2]. It is especial useful in some physical problems, plasma fusion for example, where identifying dominant low order harmonic components is essential [3]. It is conceivable that this method will play an even more important role in three dimensions not only because stacking of two dimensional slices becomes difficult if not impossible due to the constraints on viewing geometry but also because series expansion by spherical harmonics is a useful tool in many physical problems. There have been some important developments in the series expansion method in three dimensions. As in two dimensions, the analytical expressions in both real and projection spaces have been found for certain classes of radial orthogonal polynomial basis functions [4, 5, 6] and the formulas for forward and inverse transforms of general radial functions have also been derived [7]. The choice of Euler angles not only directly represents viewing geometry but also makes the angular basis functions explicitly analytical [7]. However, the above achievements have been mostly focused on the theoretical side and their numerical application has just started [8, 9]. Many practical and important aspects have yet to be explored and this is the motivation of the present paper. The major difference between the proposed method of this work and that of references [8] and [9] is that while choosing the same basis functions in the radial part, we use in the projection space the Euler angle representation in the angular part. This choice enables us to perform the least squares fit directly in the projection space and therefore no additional repeated Fourier transforms are required. This is especially useful not only in terms of saving computing time

but even more importantly, it is suitable to the cases where one has only a limited number of views, for which discrete Fourier transforms are not appropriate. We will demonstrate for the first time the applicability of this method by numerical reconstruction of a test function. The detailed algorithms and procedures are given in Section 2, the reconstruction is performed in Section 3 and Section 4 draws the conclusion.

2 Euler angle representation and series expansion

Three dimensional tomography starts from the X-ray transform of a function $f(\vec{r})$ defined by [10]

$$g(\vec{p},\hat{t}) = \int_{-\infty}^{\infty} f(\vec{p}+s\hat{t})ds \tag{1}$$

where $\hat{t}$ is a unit vector along the integration path and $\vec{p} = \vec{r} - (\vec{r}\cdot\hat{t})\hat{t}$. Hence $\vec{p} \perp \hat{t}$, where $\vec{r}$ is an arbitrary point on the integration path. In tomographic applications, $g(\vec{p},\hat{t})$ is a measured projection and $f(\vec{r})$ is the three dimensional image of interest to be reconstructed.

As shown in Figure 1, for a given integration path along a unit vector $\hat{t}$, we can always rotate the coordinate system in such a way that the new coordinate axis can be aligned as

$$\hat{z}' \parallel \hat{t}, \quad \hat{y}' \parallel \hat{p}. \tag{2}$$

It is well known that this rotation can be parameterized by the Euler angles, (α,β,γ) as shown in Figure 1. We adopt in this paper the "y convention" of Reference [11]. Using the Euler angles, a vector $\vec{x}$ in XYZ system is related to the same vector $\vec{x}'$ in $X'Y'Z'$ system by

$$\vec{x}\,' = A\vec{x}, \quad \vec{x} = A^{-1}\vec{x}\,' = A^{\top}\vec{x}\,' \tag{3}$$

where the matrix A is given by

$$A = \begin{pmatrix} \cos\alpha\cos\beta\cos\gamma - \sin\alpha\sin\gamma & \sin\alpha\cos\beta\cos\gamma + \cos\alpha\sin\gamma & -\sin\beta\cos\gamma \\ -\cos\alpha\cos\beta\sin\gamma - \sin\alpha\cos\gamma & -\sin\alpha\cos\beta\sin\gamma + \cos\alpha\cos\gamma & \sin\beta\sin\gamma \\ \cos\alpha\sin\beta & \sin\alpha\sin\beta & \cos\beta \end{pmatrix} \tag{4}$$

and

$$0 \le \alpha < 2\pi, \quad 0 \le \beta \le \pi, \quad 0 \le \gamma < 2\pi. \tag{5}$$

We can therefore always represent $\hat{t}$ and $\vec{p}$ in terms of Euler angles (α, β, γ) and $p \equiv |\vec{p}|$. Using Equation (3) their Euler angles are found to be

$$\cos\beta = \hat{t}_z \tag{6}$$

$$\cos\alpha = \frac{\hat{t}_x}{\sin\beta} \tag{7}$$

$$\sin\alpha = \frac{\hat{t}_y}{\sin\beta} \tag{8}$$

$$\sin\gamma = \frac{\hat{p}_z}{\sin\beta} \tag{9}$$

$$\cos\gamma = \frac{\hat{p}_y \sin\beta + \hat{p}_z \sin\alpha\cos\beta}{\hat{t}_x}, \tag{10}$$

when $\beta \neq 0$ and $p \neq 0$. For $\beta = 0$ we can set $\gamma = 0$ and α is determined by

$$\cos\alpha = \hat{p}_x \quad \sin\alpha = \hat{p}_y. \tag{11}$$

while for $p = 0$, γ is not needed and (α, β) are from Equations (6) to (8).

We may now rewrite Equation (1), the x-ray transform of $f(r, \theta, \phi)$, as

$$g(\vec{p}, \hat{t}) = g(p, \alpha, \beta, \gamma) = \int_{L(p,\alpha,\beta,\gamma)} f(r, \theta, \phi) ds \tag{12}$$

where $L(p, \alpha, \beta, \gamma)$ represents the integration path as shown in Figure 1.

For any given function $f(r,\theta,\phi)$ we can always make the following expansion in terms of spherical harmonics:

$$f(r,\theta,\phi) = \sum_{l=0}^{\infty}\sum_{m=0}^{l}(f_{lm}^{c}(r)S_{lm}^{c}(\theta,\phi)+f_{lm}^{s}(r)S_{lm}^{s}(\theta,\phi)) \tag{13}$$

where $f_{lm}^{c,s}(r)$ are the radial expansion components and the real spherical harmonics are simply

$$S_{lm}^{c}(\theta,\phi) \equiv Re(Y_{lm}(\theta,\phi)) = N_{lm}P_{l}^{m}(\cos\theta)\cos m\phi \tag{14}$$

$$S_{lm}^{s}(\theta,\phi) \equiv Im(Y_{lm}(\theta,\phi)) = N_{lm}P_{l}^{m}(\cos\theta)\sin m\phi \tag{15}$$

where $Y_{lm}(\theta,\phi)$ are the well known spherical harmonics defined by

$$Y_{lm}(\theta,\phi) \equiv N_{lm}P_{l}^{m}(\cos\theta)e^{im\phi} \tag{16}$$

where

$$N_{lm} \equiv (-1)^{m}\sqrt{\frac{(2l+1)(l-m)!}{4\pi(l+m)!}}, \tag{17}$$

and

$$P_{l}^{m}(x) = \frac{1}{2^{l}l!}(1-x^{2})^{m/2}\left(\frac{d}{dx}\right)^{l+m}(x^{2}-1)^{l} \tag{18}$$

is the associated Legendre function which can be rewritten in a more useful form for numerical evaluation as [12])

$$P_{l}^{m}(\cos\theta) = \frac{(l+m)!}{l!}\left(\frac{\sin\theta}{2}\right)^{m}P_{l-m}^{(m,m)}(\cos\theta) \tag{19}$$

where $P_{n}^{(\nu,\mu)}(x)$ is the Jacobi polynomial of degree n and type (ν,μ) [13].

The radial components $f_{lm}^{c,s}(r)$ also have to be expanded in terms of a complete set of basis functions $\{h_{jl}(r)\}_{j=0}^{\infty}$ (to be specified later):

$$f_{lm}^{c,s}(r) = \sum_{j=0}^{\infty}A_{jlm}^{c,s}h_{jl}(r), \tag{20}$$

where $A^{c,s}_{jlm}$ are the expansion coefficients to be determined. Equation (13) then becomes

$$f(r,\theta,\phi) = \sum_{j=0}^{\infty}\sum_{l=0}^{\infty}\sum_{m=0}^{l}(A^{c}_{jlm}S^{c}_{lm}(\theta,\phi)+A^{s}_{jlm}S^{s}_{lm}(\theta,\phi))h_{jl}(r) \tag{21}$$

We define $W^{c,s}_{jlm}(\alpha,\beta,\gamma,p)$ as follows and it has been proven that [7]

$$W^{c,s}_{jlm}(\alpha,\beta,\gamma,p)\equiv\int_{L(p,\alpha,\beta,\gamma)}dsS^{c,s}_{lm}(\theta,\phi)h_{jl}(r)=\sum_{m'=0}^{l}V^{c,s}_{lmm'}(\alpha,\beta,\gamma)g_{jlm'}(p) \tag{22}$$

where

$$\begin{aligned}V^{c}_{lmm'}(\alpha,\beta,\gamma) &= \delta_{m'}\Big[\cos(m\alpha+m'(\gamma+\pi/2))d^{(l)}_{mm'}(\beta)\\ &\quad +(-1)^{m'}(\cos(m\alpha-m'(\gamma+\pi/2))d^{(l)}_{m,-m'}(\beta)\Big]\end{aligned} \tag{23}$$

$$\begin{aligned}V^{s}_{lmm'}(\alpha,\beta,\gamma) &= \delta_{m'}\Big[\sin(m\alpha+m'(\gamma+\pi/2))d^{(l)}_{mm'}(\beta)\\ &\quad +(-1)^{m'}(\sin(m\alpha-m'(\gamma+\pi/2))d^{(l)}_{m,-m'}(\beta)\Big]\end{aligned} \tag{24}$$

where

$$\delta_m=\begin{cases}1/2 & m=0\\ 1 & m\neq 0\end{cases} \tag{25}$$

and

$$d^{(l)}_{mm'}(\beta)\equiv\sqrt{\frac{(l+m')!(l-m')!}{(l+m)!(l-m)!}}\left(\sin\frac{\beta}{2}\right)^{m'-m}\left(\cos\frac{\beta}{2}\right)^{m'+m}P^{(m'-m,m'+m)}_{l-m'}(\cos\beta) \tag{26}$$

(for $m'\geq m$)

and

$$d^{(l)}_{mm'}(\beta)=(-1)^{m-m'}d^{(l)}_{m'm}(\beta)\quad(\text{for }\ m\geq m'), \tag{27}$$

and $g_{jlm}(p)$ are the radial basis functions in the projection space (α,β,γ,p), obtained from $h_{jl}(r)$ by [7]

$$g_{jlm}(p)=N_{lm}(1+(-1)^{l+m})\int_p^1\frac{rdrh_{jl}(r)}{\sqrt{r^2-p^2}}P^m_l\left(\sqrt{1-\left(\frac{p}{r}\right)^2}\right). \tag{28}$$

Taking the x-ray transform of $f(r,\theta,\phi)$ in Equation (21) and employing Equation (22) we can therefore expand the projection $g(\alpha,\beta,\gamma,p)$ defined in Equation (12) as

$$g(\alpha,\beta,\gamma,p)=\sum_{j=0}^{\infty}\sum_{l=0}^{\infty}\sum_{m=0}^{l}(A^c_{jlm}W^c_{jlm}(\alpha,\beta,\gamma,p)+A^s_{jlm}W^s_{jlm}(\alpha,\beta,\gamma,p)). \tag{29}$$

So far we have not specified $h_{jl}(r)$ yet. In principle once it is given, by a certain physical model for example, one can always use Equation (28) to get $g_{jlm}(p)$ at least by numerical integration. In this paper, we choose the orthogonal polynomials

$$h_{jl}(r)=r^l(1-r^2)P_j^{(l+1/2,1)}(1-2r^2), \tag{30}$$

because its $g_{jlm}(p)$ can be carried out analytically [4, 6], namely

$$g_{jlm}(p)=\begin{cases} G_{jlm}p^m(1-p^2)^{3/2}P^{(m,3/2)}_{(l-m)/2+j}(1-2p^2) & l+m=even \\ 0 & l+m=odd, \end{cases} \tag{31}$$

where

$$G_{jlm}\equiv\frac{(-1)^l(j+1)(\frac{l-m}{2}+j)!\sqrt{(2l+1)(l-m)!(l+m)!}}{2^{l+1}\Gamma(\frac{l-m}{2}+j+2+\frac{1}{2})\left(\frac{l-m}{2}\right)!\left(\frac{l+m}{2}\right)!}. \tag{32}$$

It should be noted that although the above formulas look complicated, the only special function which appears in Equations (19), (30), (31) and (26) is the Jacobi polynomial $P_n^{(\nu,\mu)}(x)$. Its evaluation can be performed by using the stable recursion formula suggested by Abramowitz and Stegun (Eq. 22.7.1 of [13]) that

$$\begin{aligned} & 2(n+1)(n+\nu+\mu+1)(2n+\nu+\mu)P^{(\nu,\mu)}_{n+1}(x) \\ = \; & [(2n+\nu+\mu+1)(\nu^2-\mu^2)+(2n+\nu+\mu)(2n+\nu+\mu+1)(2n+nu\mu+2)x]P^{(\nu,\mu)}_n(x) \\ & -2(n+\nu)(n+\mu)(2n+\nu+\mu+2)P^{(\nu,\mu)}_{n-1}(x) \end{aligned} \tag{33}$$

with

$$P_0^{(\nu,\mu)}(x)=1, \quad \text{and} \quad P_1^{(\nu,\mu)}(x)=[\nu-\mu+(\nu+\mu+2)x]/2. \tag{34}$$

3 Reconstruction

We take the following function with an ellipsoidal iso-valued surface as our test function

$$f^t(x,y,z) = \exp\left\{-\left(\frac{x^2}{a^2}+\frac{y^2}{b^2}+\frac{z^2}{c^2}\right)\right\} \tag{35}$$

$$\text{where} \quad a = 0.2 \quad b = 0.3 \quad c = 0.4$$

and its projection $g^t(\alpha,\beta,\gamma,p)$ is from the numerical integration, Equation (12).

In our simulation, 21 x 21 element array detectors are used. We have two detection setups. There are four arrays in the first setup. They are located symmetrically at the four corners of an equal-sided tetrahedron which is centered at the origin of a coordinate system. The straight line through the center and each corner of the tetrahedron passes through the center of each array and is normal to it as well. Each array receives signals through a pin hole aperture. The maximum chord distance, p, is about one. In the second case, the setup is the same except four more arrays are added. The eight arrays are now located symmetrically at the eight corners of a cube.

The number of series expansion terms in Equations (21) and (29) is infinite, however in practical applications the number of measured projections is finite, and therefore the series has to be truncated. After a proper truncation we have

$$f(r,\theta,\phi) = \sum_{j=0}^{J}\sum_{l=0}^{L}\sum_{m=0}^{l}(A^c_{jlm}S^c_{lm}(\theta,\phi) + A^s_{jlm}S^s_{lm}(\theta,\phi))h_{jl}(r) \tag{36}$$

and

$$g^t(\alpha_k,\beta_k,\gamma_k,p_k) = \sum_{j=0}^{J}\sum_{l=0}^{L}\sum_{m=0}^{l}(A^c_{jlm}W^c_{jlm}(\alpha_k,\beta_k,\gamma_k,p_k) + A^s_{jlm}W^s_{jlm}(\alpha_k,\beta_k,\gamma_k,p_k)) \tag{37}$$

$$k = 1,2,\cdots,N.$$

where N is the total number of measurements. Equations (37) are just linear equations for the unknowns $A^{c,s}_{jlm}$ and this system can be solved by the method of least squares. If the samples are

equally or approximately equally spaced then the Nyquist principle can be used to estimate the maximum number of expansion harmonics which may be resolved [3]. However, this is not the case in our sample space, at least in the angular subspace (α, β, γ). How to directly determine the truncation in this case is still an open question and therefore numerical reconstruction tests were conducted in lieu of this. We have found by trial and error that

$$L = 3 \quad J = 9 \ \text{(for 4 arrays)} \ \text{and} \quad L = 6 \quad J = 9 \ \text{(for 8 arrays)} \tag{38}$$

gives optimal reconstruction results. We'd like to point out that the maximum radial number, $J = 9$, from numerical tests does agree with what the Nyquist principle requires; namely that the number of samples should be at least twice the frequency of the highest spatial harmonics in the radial direction. In our detector geometry (21 samples in roughly radial direction), the chord radial spacing is uniform enough to apply the Nyquist theorem. (This points out another one of the reasons for deriving this analytical expansion technique — the radial and angular parts of the transform problem are separable.)

After solving Equation (37) for the expansion coefficients, $A^{c,s}_{jlm}$, the reconstructed function is then given by Equation (36). In Figure 2 (4 array case) and Figure 3 (8 array case) we show a few three dimensional iso-valued surfaces of the reconstructed function in comparison with that of the test function. As one can see while the reconstruction is reasonably good for the case with four arrays it is greatly improved when eight arrays are used. The slight deformation of the surfaces in Figure 2 is due to the fact that, although the test function Equation (35) looks simple, it does contain an infinite number of spherical harmonics. This can be seen by rewriting $f^t(x, y, z)$ in spherical coordinates as

$$f^t(r, \theta, \phi) = \exp\left\{-r^2\left(\frac{(\cos\phi\sin\theta)^2}{a^2} + \frac{(\sin\phi\sin\theta)^2}{b^2} + \frac{(\cos\theta)^2}{c^2}\right)\right\} \tag{39}$$

and making the expansion $e^{-z} = 1 - z + z^2/2 + \cdots$. It is immediately clear that higher harmonics are there, especially at large radii. The slight deformation is an "aliasing" effect, which shows up as expected as a result of not having a sufficient number of samples.

4 Conclusion

We have presented a series expansion method in which the Euler angles and orthogonal polynomials were employed. We have also show the detail algorithms and procedures of the method. The applicability is demonstrated through a successful reconstruction of a test function. We hope to see the use of this method to a real problem in the field of plasma physics, for example laser fusion [14, 15], in the near future.

Acknowledgements

We wish to thank Professor Ian Hutchinson for his valuable suggestions.

References

[1] A. M. Cormack, *Representation of a function by its line integrals, with some radiological applications,* J. Appl. Phys., 10 (1964), pp. 2908-2913.

[2] S. R. Deans, *A unified Radon inversion formula,* J. Math. Phys., 19 (1978), pp. 2346-2349.

[3] R. S. Granetz, P. Smeulders, X-ray tomography on Jet, Nuclear Fusion, 28 (1988), pp. 457-476.

[4] P. Maass, *The X-ray transform: singular value decomposition and resolution,* Inverse Problems 3 (1987), pp. 727-741.

[5] S. H. Izen, *A series inversion for the X-ray transform in n dimensions,* Inverse Problems, 4 (1988), pp. 725-748.

[6] S. H. Izen, *Inversion of the k-plane transform by orthogonal function series expansions,* Inverse Problems, 4 (1988), pp. 725-748.

[7] L. Wang *The X-ray transform and its inversion for the series expansion basis functions in three dimensional tomography,* to appear on SIAM, J. Math. Anal., 52 (1992). (Oct. Issue 5)

[8] S. H. Izen, *An application for a limited solid angle x-ray transform,* Contemporary Mathematics, 113 (1990), pp. 151-170.

[9] S. H. Izen, *Inversion of the x-ray transform from data in a limited angular range,* in Signal Processing, Part 2, IMA Volumes in Mathematics and its Applications #23, Springer Verlag, 1990.

[10] D. C. Solmon, *The X-ray transform,* J. Math. Anal. Appl., 56 (1976), pp. 61-83.

[11] H. Goldstein, *Classical mechanics,* Addison-Wesley, Mass, 1980.

[12] L. C. Biedenharn and J. D. Louck, *Encyclopedia of Mathematics and its applications. Vol.8: Angular Momentum in Quantum Physics,* Adison-Wesley, Mass., 1981.

[13] M. Abramowitz and I. A. Stegun, *Handbook of Mathematical Functions,* Dover Publications, New York, 1970.

[14] M. Nakai, et al, *Development of x-ray emission computed tomography for ICF research,* Rev. Sci. Instrum. 61 (1990) pp. 2783-2785.

[15] Y. W. Chen, et al, *Three-dimensional imaging of laser imploded targets,* J. Appl. Phys. 68 (1990) pp. 1483-1488.

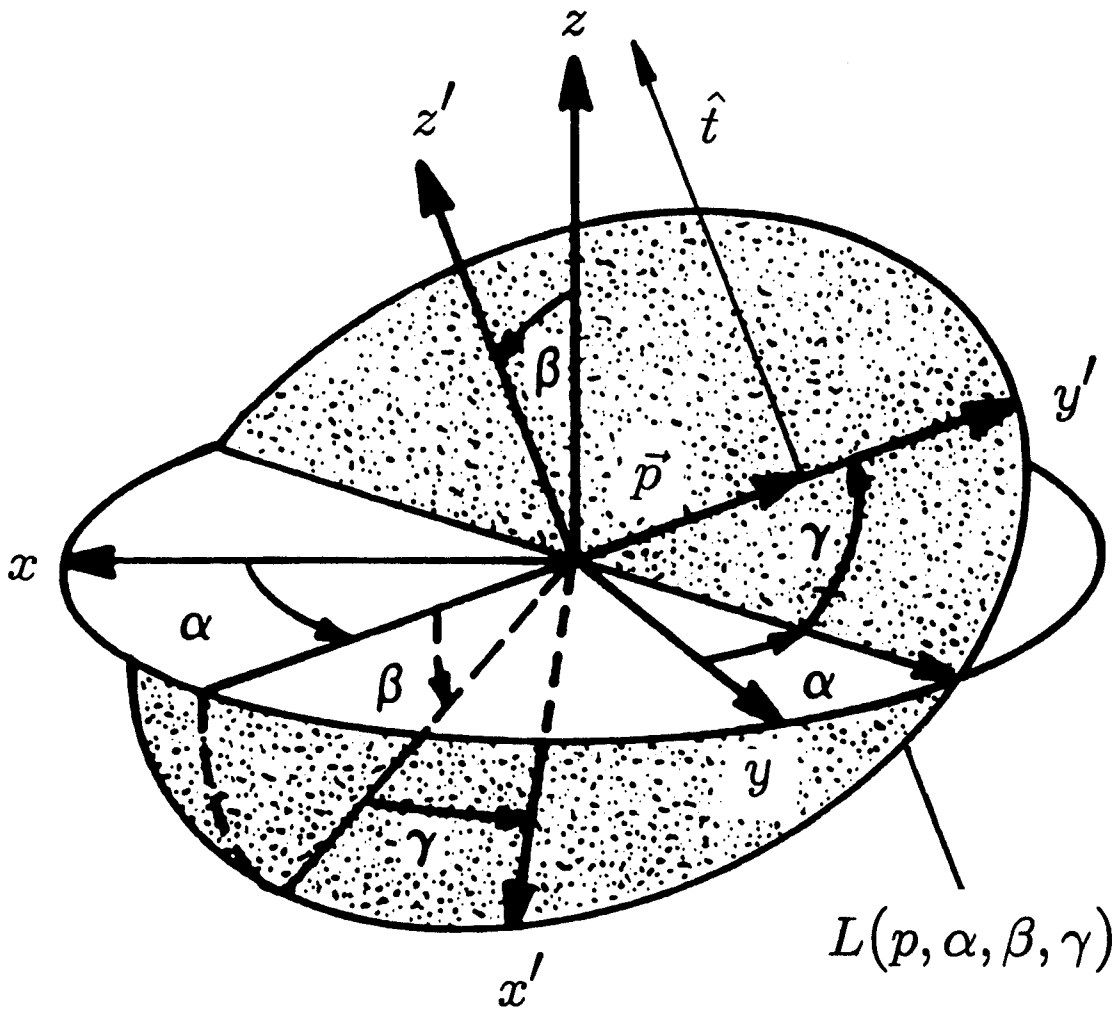

FIG. 1. The Euler angle representation of the integration path $L(p, \alpha, \beta, \gamma)$.

Reconstructed function Test function

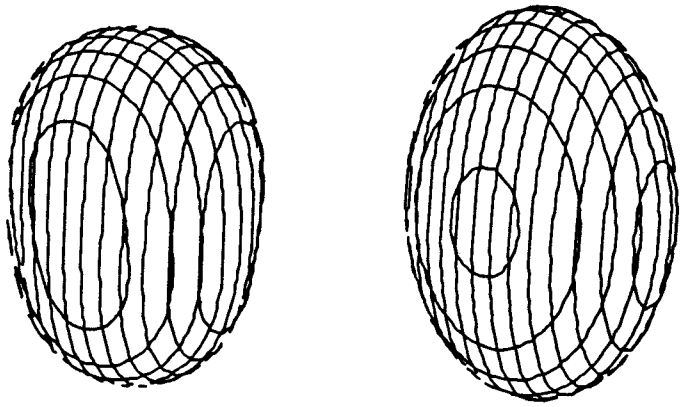

A. $f(r,\theta,\phi) = 0.4$ surface

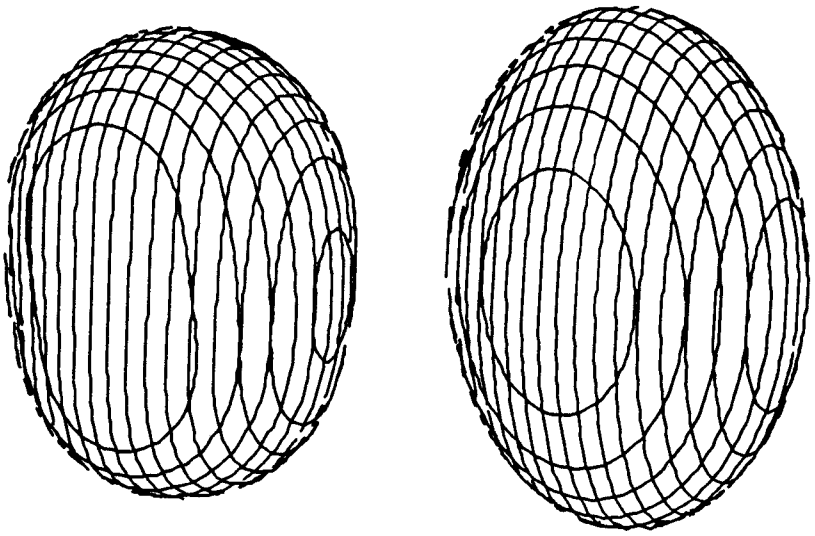

B. $f(r,\theta,\phi) = 0.2$ surface

FIG. 2. 3-D iso-valued surfaces of the reconstructed function (left) and test function (right) when 4 arrays are used.

Reconstructed function Test function

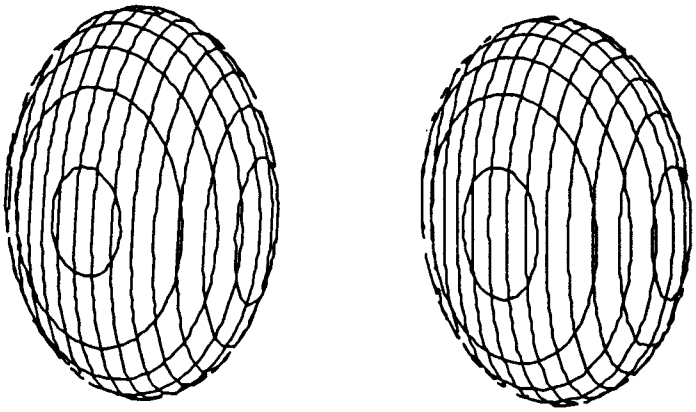

A. $f(r, \theta, \phi) = 0.4$ surface

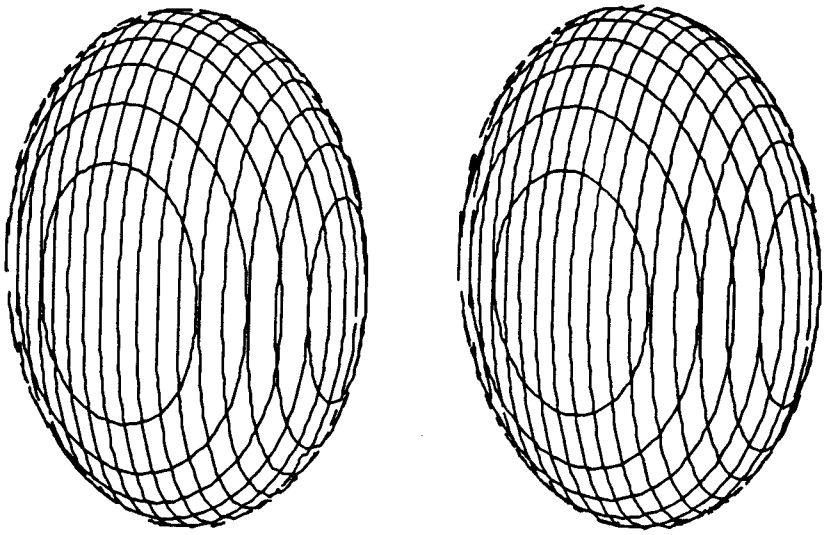

B. $f(r, \theta, \phi) = 0.2$ surface

FIG. 3. 3-D iso-valued surfaces of the reconstructed function (left) and test function (right) when 8 arrays are used.